Optical Microwave Waveforms Generation Based on the Round-Trip Phase of the DFB Laser

Congbiao Lei, Wenyang Yuan, Guangcheng Zhong, Yuxuan Jiang, Mingqi Jiao, Jiaqi Yao, and Liang Xie

***Abstract*—In this paper, we theoretically and experimentally analyze the influence of the round-trip phase of distributed feedback (DFB) lasers on the harmonic-phase of photocurrent, caused by the external injection current. The results indicate that the harmonic-phase of photocurrent introduced by the round-trip phase (HPIRP) reduces with the increase of modulation depth at a fixed frequency. Then, based on the HPIRP of the DFB laser, a simple photonic generation method of optical microwave waveforms is proposed and verified. In this scheme, three lasers with different wavelengths are mainly used. By adjusting the tunable optical delay lines and attenuators, the amplitude and phase of the photocurrent of the three branches converted by the photodetector (PD) can be controlled individually. The photocurrent of the superposition of the three branches can be controlled properly to form the target waveform. Dispersive elements and complex microwave photonic filtering are not required. Through experiments, rectangular and triangular waveforms with a repetition frequency of 3.75 GHz are generated.**

***Index Terms*—DFB laser, microwave photonics, optical microwave waveforms.**

I. Introduction

PHOTONIC generation of microwave waveforms has been widely studied and has broad application prospects in radar, signal processing, wireless communications, and modern instrument testing [1], [2], [3]. Optical microwave waveforms can break through the bandwidth limitation of electronic devices and can take advantage of the anti-electromagnetic interference and low loss of optical fiber transmission.

Recently, researchers have proposed a variety of methods for generating photonic microwave waveforms based on external modulators. In Ref [4], variable photonic microwave waveforms generation is achieved by controlling the radio frequency (RF) signals and direct current (DC) bias voltages of dual-parallel Mach-Zehnder modulator (DPMZM). This method does not require dispersive components and photonic filtering. In Ref [5], frequency-doubled triangular, rectangular, sawtooth waveforms, and triangle waveforms with adjustable symmetry are generated based on simulation. A Mach-Zehnder modulator (MZM) performs carrier suppression modulation to produce a dual-frequency optical signal. The DPMZM generates ±1st, ±3rd-order sidebands. A second MZM generates ±2nd-order sidebands. After the balance detector conversion, 2nd-order, 4th-order, and 6th-order harmonics are generated to synthesize frequency-double photonic microwave waveforms. This principle is complex and has not been verified experimentally. In Ref [6], Wang et al. generate a triangular waveform using a dual-polarization quadrature phase-shift-keying (DP-QPSK) modulator. The repetition rate of the triangular waveform is four times the RF signal. The modulation index of this method is flexible and adjustable, which increases the flexibility of the system. However, the phase noise of the frequency tripler will cause drifting of the harmonics and affect the quality of the waveform. In Ref [7], Zhu et al. use a single MZM to realize the generation of optical rectangular and triangular waveforms. However, a 90° mixing coupler is used for phase modulation to generate a triangular waveform, which reduces the flexibility of the system. In Ref [8], a photonic generation scheme of square and triangular waveforms with tunable duty cycles is proposed based a single MZM. By adjusting the magnitude of the second harmonic amplitude, the duty cycles of the triangle and square microwave waveforms are controlled. However, this method is polarization-dependent, and it is necessary to control the polarization of the two optical paths to ensure the stability of the system. In Ref [9], pulse shaping is performed by two cascaded single-drive lithium niobate MZMs. The polarization state of the incident light should be controlled so that two independent sidebands with orthogonal polarizations are obtained in the optical field. Rectangular waveform, triangular waveform, sawtooth and reversed-sawtooth waveform are obtained through the superposition of the orthogonal signals. Polarization-dependent also reduces the stability of the scheme. At the same time, two MZMs increase the complexity and cost of the system.

External modulators require continuous wave (CW) lasers to generate optical carriers. The DC bias drift of the MZM modulators can result in undesired waveforms [4], [5], [6], [7], [8], [9]. In Ref [4], [5], [9], the schemes are polarization-dependent, which will reduce the stability of the system. In this letter, a method of photonic microwave waveform generation based on directly modulated DFB lasers is proposed. Directly modulated DFB laser is both a light source and a modulation device, with the advantages of low threshold current, compact structure, and low cost. The previous methods of photonic microwave waveforms generation based on external modulators just regulate the

Manuscript received 27 November 2022; revised 4 January 2023; accepted 15 January 2023. Date of publication 20 January 2023; date of current version 1 February 2023. This work was supported by the Scientific Instrument Developing Project of the Chinese Academy of Sciences under Grant YJKYYQ20200056. *(Corresponding author: Liang Xie.)*

The authors are with the State Key Laboratory on Integrated Optoelectronics, Institute of Semiconductors, Chinese Academy of Sciences, Beijing 100083, China and also with the College of Materials Science and Opto-Electronic Technology, University of Chinese Academy of Sciences, Beijing 100049, China (e-mail: leicongbiao@semi.ac.cn; ywysjl@semi.ac.cn; zhonggc@semi.ac.cn; jiangyuxuan@semi.ac.cn; jmq@semi.ac.cn; yaojiaqi@semi.ac.cn; xiel@semi.ac.cn).

Digital Object Identifier 10.1109/JPHOT.2023.3238133

amplitude of the harmonics. In this letter, The scheme proposed adjusts the amplitude and phase of the harmonics at the same time, which can generate the target waveform more accurately.

In this letter, the influence of the round-trip phase of DFB lasers on the harmonic phase of photocurrent is analyzed theoretically and experimentally. The experiment results indicate the existence of HPIRP, which can be reduced by controlling the modulation depth. Based on this theory, a flexible method of optical microwave waveforms generation is proposed and experimentally verified. Photonic triangular and rectangular waveforms with a repetition frequency of 3.75 GHz are obtained successfully.

II. Theory Analysis

DFB lasers are widely used in the fields of 5G communication and analog optical communication [10], [11]. However, the frequency chirp and nonlinear of the DFB laser will cause serious signal distortion [12], [13], limiting the application scenarios of DFB lasers.

DFB laser is an optoelectronic device, and the external injection current will change the carrier concentration in the active region, which will cause changes in the effective refractive index. The relationship between the effective refractive index of the active region and the carrier concentration is expressed as [14]:

$$n_{eff} = n_{th} - \frac{\lambda_{br}}{4\pi}\Gamma\alpha\frac{dg}{dN}(N - N_{th}) \tag{1}$$

where λ_{br} is the Bragg wavelength, Γ denotes the optical confinement factor, $\alpha$is the linewidth enhancement factor, dg/dN is the differential gain. When the optical field propagates in the resonant cavity of the DFB laser, the variation of n_{eff} will result in different round-trip phases ϕ_{eff}. The round-trip phase ϕ_{eff}has a relationship with the effective refractive index n_{eff} and the Bragg wavelength λ_{br}.

$$\frac{d\phi_{\text{eff}}}{dn_{eff}} \cong -2\frac{c_0}{n_{eff}} \cdot T_{\text{eff}} \cdot \frac{2\pi}{\lambda_{br}} \tag{2}$$

where c_0 is the vacuum velocity of light, T_{eff} is the effective round-trip time. Eq. (2) indicates that the emission wavelength differs from the Bragg wavelength will result in different round-trip phases. The optical carrier and modulation sidebands will have different original phases. After square law detection of PD, harmonics of the photocurrent of PD output will have different original phases.

Following, the HPIRP of photocurrent will be analyzed theoretically. Assuming the light field of DFB laser output is:

$$E(t) = E_0\cos(\omega_0 t + \varphi_0) \tag{3}$$

where A_0 is the amplitude of the light field, ω_0 is the angular frequency, and φ_0 is the original phase. The modulation signal is expressed as:

$$a(t) = A_m\cos(\omega_m t) \tag{4}$$

where A_m and ω_m are the amplitude and angular frequency of the RF signal, respectively.

When the RF signal is applied to the DFB laser, modulation sidebands of the light field will be generated. The expression of the modulated light field is given by:

$$\begin{aligned} E_m(t) &= A_0[1 + m_a\cos(\omega_m t)] \cdot \cos(\omega_0 t + \varphi_0) \\ &= A_0\cos(\omega_0 t + \varphi_0) + \frac{m_a}{2}A_0\cos[(\omega_0 + \omega_m)t + \varphi_0] \\ &\quad + \frac{m_a}{2}A_0\cos[(\omega_0 - \omega_m)t + \varphi_0] \end{aligned} \tag{5}$$

where $m_a = A_m/A_0$ denotes the modulation depth.

Due to the difference in the round-trip phase ϕ_{eff} of the optical carrier and sidebands, the modified expression of the light field of the DFB laser is given by:

$$\begin{aligned} E_m(t) =& A_0\cos(\omega_0 t+\varphi_0)+\frac{m_a}{2}A_0\cos[(\omega_0+\omega_m)t+\varphi_0+\theta_{+1}] \\ &+ \frac{m_a}{2}A_0\cos[(\omega_0 - \omega_m)t + \varphi_0 + \theta_{-1}] + \ldots \end{aligned} \tag{6}$$

where $\theta_{\pm1}$ is the phase introduced by the round-trip phase. Due to the phase difference between the carrier and sidebands, the harmonics of the photocurrent have different HPIRPs, and the photocurrent converted by PD can be expressed as:

$$\begin{aligned} i(t) &\propto \frac{1}{T}\int_0^T E_m(t-\tau)\cdot E_m(t-\tau)dt \\ &= \frac{1}{2}\left(A_0^2 + \frac{m_a^2}{2}A_0^2\right) + \frac{m_a}{4}A_0^2\cos(\omega_m t - \omega_m\tau + \theta_{+1}) \\ &\quad + \frac{m_a}{4}A_0^2\cos(\omega_m t - \omega_m\tau - \theta_{-1}) \\ &\quad + \frac{m_a}{8}A_0^2\cos(2\omega_m t - 2\omega_m\tau + \theta_{+1} - \theta_{-1}) \\ &\propto a_1\cos(\omega_m t - \omega_m\tau) + a_2\cos(2\omega_m t - 2\omega_m\tau + \psi_2) \\ &\quad + a_3\cos(3\omega_m t - 3\omega_m\tau + \psi_3) + \ldots \end{aligned} \tag{7}$$

where a_n is the amplitude of nth-order harmonic, $\tau$is the delay time of optical fiber, and ψ_n is HPIRP of nth-order harmonic of photocurrent.

III. Experiment and Discussion

The following experiments analyze the HPIRP at different modulation frequencies and different modulation depths. A homemade butterfly-packaged laser is used, with a threshold current of 15 mA, a center wavelength of 1310.15 nm at 30 mA, and a 3 dB bandwidth of 15 GHz at 30 mA.

The experimental setup is shown in Fig. 1. The laser is driven by a current source (Keithley 2400). The optical signal is converted to an electric signal by a high-speed photodetector (XPDV2320R) with a bandwidth of 50 GHz. The time-domain waveform is measured by an oscilloscope (DPO70000). The power spectrum is monitored through an electrical spectrum analyzer (FSWP).

The modulation depth of the laser is defined as: I_{RF}/I_{bias}. I_{RF} is the amplitude of the RF signal and I_{bias} is the bias current. To study the relationship between modulation depth and HPIRP of the DFB laser, the laser is driven by RF signal at frequencies of 4 GHz, 6 GHz, 8 GHz, and 10 GHz respectively. The power of the RF signal is fixed at 10 dBm. The modulation depth is changed along with the variation of the bias current. The power

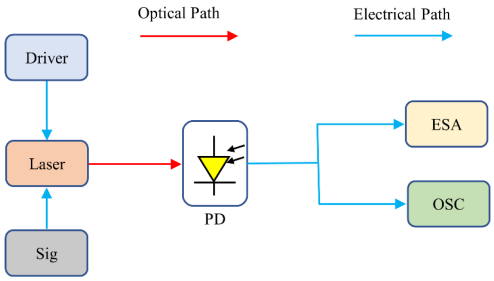

Fig. 1. Experimental setup of laser testing. Sig: signal generator; PD: high-speed photodetector; ESA: electrical spectrum analyzer. OSC: oscilloscope.

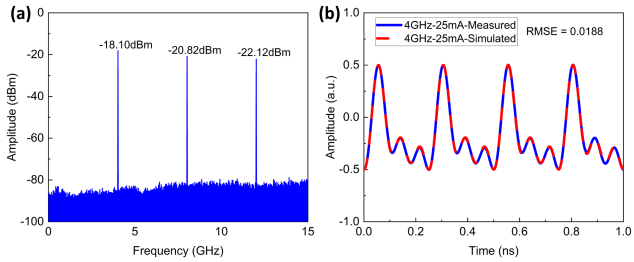

Fig. 2. (a) The power spectrum of the DFB laser. (b) The measured and simulated time-domain waveform, with a bias current of 25 mA and RF signal of 4 GHz and 10 dBm.

spectrum of photocurrent is observed by the electrical spectrum analyzer. To simplify the experiments, the harmonics above the third-order harmonic are filtered out by a low pass filter within the oscilloscope. The generated waveforms of the superposition of the first three harmonics of the photocurrent are captured by the oscilloscope.

The time-domain waveform can be expressed as the sum of Cosine functions in (7). a_n is the amplitude of the nth-order harmonic detected on the electrical spectrum analyzer. The power spectrum of photocurrent is shown in Fig. 2(a), when the DFB laser is biased at 25 mA and driven by an RF signal of 4 GHz and 10 dBm. a_n in (7) can be obtained from the power spectrum as: $a_1 = 0.0394$, $a_2 = 0.0288$, $a_3 = 0.0248$. The time-domain waveform is shown in Fig. 2(b). By least squares curve fitting between the measured waveform and the simulated waveform of (7), HPIRP of the second-order harmonic and third-order harmonic are obtained as: $\Psi_2 = 0.4249rad$, $\Psi_3 = 0.7393rad$. The root mean square error (RMSE) between the measured waveform and the simulated waveform is 0.0188.

The phase under other conditions is obtained by the same method. Fig. 3 shows the relationship between the HPIRP of harmonics and the bias current at different frequencies. When the bias current increases (the modulation depth decreases), the HPIRP gradually become larger. And the HRIRP of the second-order harmonic is smaller than that of the third-order harmonic.

Modulation depth can also be controlled by changing the power of the RF signal with a fixed bias current. Fig. 4 shows the relationship between HPIRP and the power of RF signals of 4, 6, 8, and 10 GHz, respectively. The DFB laser is biased at 25 mA. It can be seen from Fig. 4 that HPIRP decreases with the

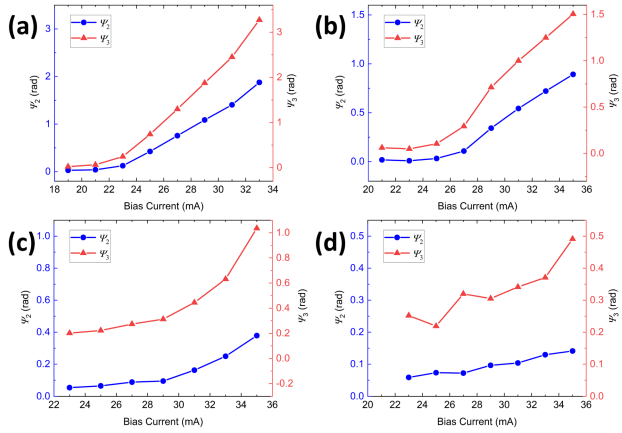

Fig. 3. The relationship between HRIRP and bias current at the frequency of (a) 4 GHz; (b) 6 GHz; (c) 8 GHz; (d) 10 GHz, with a RF signal of 10 dBm.

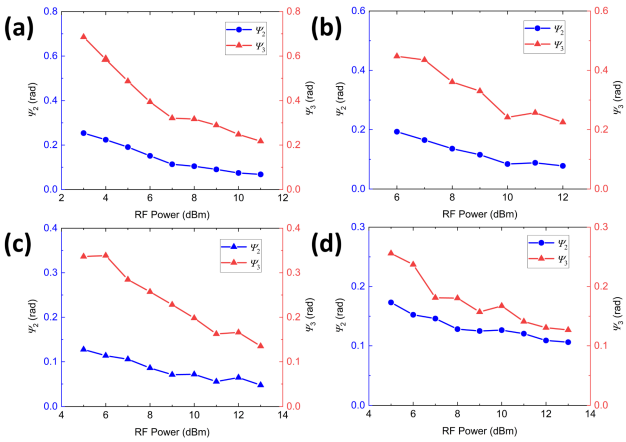

Fig. 4. The relationship between HPIRP and RF power at the frequency of (a) 4 GHz; (b) 6 GHz; (c) 8 GHz; (d) 10 GHz, with a bias current of 25 mA.

increase of the modulation depth (the increase of the RF power), which is consistent with the above analysis.

The above analysis shows that the round-trip phase of the DFB laser will cause HPIRP. The HPIRP decreases with the increase of modulation depth. By properly designing, HPIRP can be used to generate optical microwave waveforms.

IV. Generation of Optical Microwave Waveforms

A. Triangular Waveform

Theoretical research shows that optical triangular and rectangular waveforms can be synthesized through the first two items of the Fourier expansion [14]. The Fourier expansion of a triangular waveform is given by:

$$T_{tri}(t) = C_0 + \sum_{n=1,3,5,\ldots}^{\infty} \frac{1}{n^2}\cos[n(\omega t + \varphi)]$$

$$\approx C_0 + \cos(\omega t + \varphi) + \frac{1}{9}\cos[3(\omega t + \varphi)] \quad (8)$$

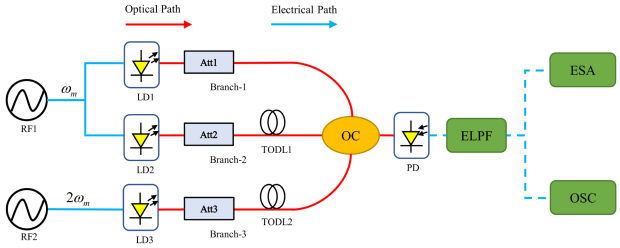

Fig. 5. Schematic diagram of the experimental setup. LD: laser diode; TODL: tunable optical delay line; OC: optical coupler; PD: photodetector; ELPF: electrical low-pass filter; ESA: electrical spectrum analyzer; OSC: oscilloscope.

By adjusting the amplitude and phase of the fundamental tone and the third-order harmonic, a photonic triangular waveform can be obtained through the superimposition of the photocurrent of the three branches. The schematic diagram is shown in Fig. 5.

The RF signal 1 (RF1) of 3.75 GHz is divided into two branches, which are applied to laser diode-1 (LD1) and LD2 respectively. LD3 is driven by RF signal 2 (RF2) of 7.5 GHz. The tunable optical delay lines control the phase difference between the three branches. The attenuators control the amplitudes of the optical carrier and sidebands. Three lasers with different wavelengths are used to avoid interference. After the square-law detection of PD, the harmonics above the third-order harmonic of the photocurrent are filtered out through an ELPF. The harmonics of the photocurrents generated by the three lasers are given by the following equations:

$$\begin{cases} i_1(t) = a_{11}\cos[\omega_m(t-\tau_1)] + a_{12}\cos[2\omega_m(t-\tau_1)+\psi_{12}] \\ \qquad +a_{13}\cos[3\omega_m(t-\tau_1)+\psi_{13}] \\ i_2(t) = a_{21}\cos[\omega_m(t-\tau_2)] + a_{22}\cos[2\omega_m(t-\tau_2)+\psi_{22}] \\ \qquad +a_{23}\cos[3\omega_m(t-\tau_2)+\psi_{23}] \\ i_3(t) = a_{31}\cos[2\omega_m(t-\tau_3)] \end{cases} \tag{9}$$

The optical signals of the three branches are combined by an optical coupler. The photocurrent of the superposition of the three branches can be expressed as:

$$i(t) = i_1(t) + i_2(t) + i_3(t) \tag{10}$$

By properly controlling the delay time and attenuation of the three branches, the amplitude and phase of the photocurrents of the three lasers can be controlled individually. The relationship ($a_1/a_3 = 9$, $a_2 = 0$) of the Fourier series of the triangular waveform can be achieved.

The power spectrum of branch-1 measured by ESA and the time-domain waveform captured by OSC are shown in Fig. 6(a) and (b). HPIRPs of the second-order and the third-order harmonic are obtained by least squares curve fitting as: $\Psi_{12} = 0.7512rad$, $\Psi_{13} = 1.1503rad$.

The photocurrent of branch-1 converted by PD can be expressed as:

$$i_1(t) = a_{11}\cos[\omega_m(t-\tau_1)] + a_{12}\cos[2\omega_m(t-\tau_1)+0.7512] + a_{13}\cos[3\omega_m(t-\tau_1)+1.1503] \tag{11}$$

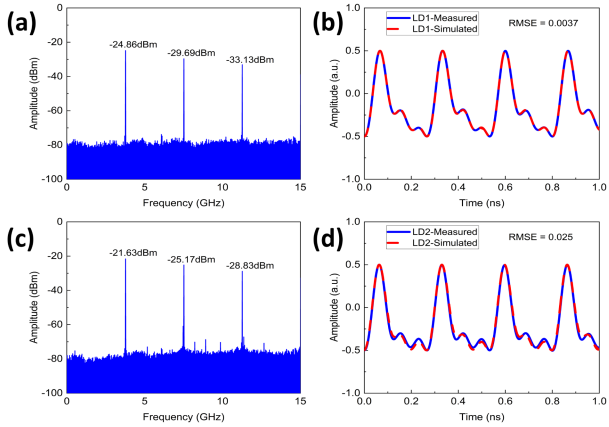

Fig. 6. (a) The power spectrum of branch-1. (b) The measured and simulated waveforms of branch-1. (c) The power spectrum of branch-2. (d) The measured and simulated waveforms of branch-2.

The power spectrum and time-domain waveform of branch-2 are shown in Fig. 6(c) and (d). HPIRPs of branch-2 are: $\Psi_{22} = 0.2604rad$, $\Psi_{23} = 0.5059rad$.

The photocurrent of branch-2 can be expressed as:

$$i_2(t) = a_{21}\cos[\omega_m(t-\tau_2)] + a_{22}\cos[2\omega_m(t-\tau_2)+0.2604] + a_{23}\cos[3\omega_m(t-\tau_2)+0.5059] \tag{12}$$

To satisfy the amplitude and phase requirements of the triangular waveform, the delay time of branch-2 should be set as $\tau_2 = \tau_1 + [(2n+1)\pi + 0.77]/\omega_m$. The photocurrent of the branch-2 becomes:

$$\begin{aligned} i_2(t) = & -a_{21}\cos[\omega_m(t-\tau_1) - 0.77] + a_{22}\cos[2\omega_m(t \\ & -\tau_1) + 0.2604] \\ & -a_{23}\cos[3\omega_m(t \\ & -\tau_1) + 1.2759] \end{aligned} \tag{13}$$

The sum of the photocurrent of branch-1 and branch-2 is calculated mathematically. Assuming that the second-order harmonic has been filtered out. The expressions of the fundamental tone, the third-order harmonic, and the superposition are shown in (14).

$$\begin{cases} i_{fund} = a_{11}\cos[\omega_m(t-\tau_{11})] - a_{21}\cos[\omega_m(t-\tau_1) - 0.77] \\ i_{thir} = a_{13}\cos[3\omega_m(t-\tau_{13}) + 1.1503] - a_{23}\cos[3\omega_m(t \\ \qquad -\tau_1) + 1.2759] \\ i_{tri} = i_{fund} + i_{thir} \end{cases} \tag{14}$$

The simulated waveforms are shown in Fig. 7. The amplitude of the fundamental tone is 8.62 times larger than that of the third-order harmonic, which is very close to the ideal ratio of 9. The fundamental tone and the third-order harmonic are phase-matched to synthesize a triangular waveform. As shown in Fig. 7, a simulated triangular waveform is obtained. The RMSE between the simulated triangular waveform and the ideal waveform is 0.0342.

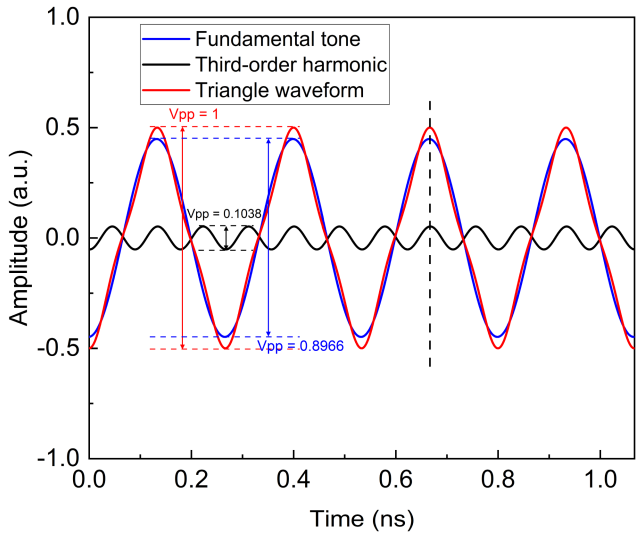

Fig. 7. The simulation of photonic generation of triangular waveform.

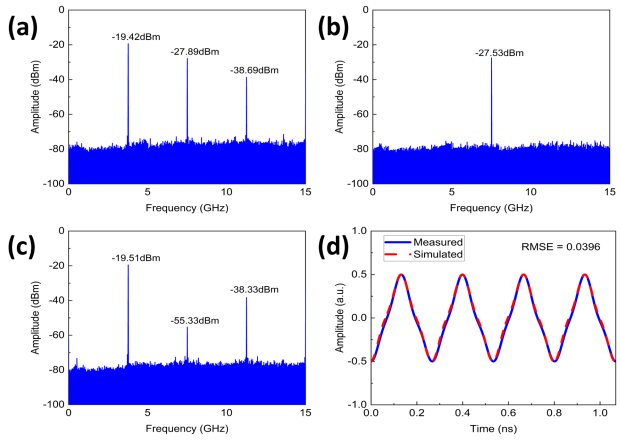

Fig. 8. (a) The power spectrum of the superposition of branch-1 and branch-2. (b) The power spectrum of branch-3. (c) The power spectrum of the superposition of the three branches. (d) The measured and simulated triangular waveforms.

A proof-of-concept experiment is carried out to verify the simulated triangular waveform. By properly adjusting TODL2, the delay time of $\tau_2 = \tau_1 + [(2n+1)\pi + 0.77]/\omega_m$ can be made. The power spectrum of the sum of branch-1 and branch-2 is shown in Fig. 8(a). The power of the third-order harmonic is 18.82 dB lower than that of the fundamental tone, which is close to the theoretical value of 19.08 dB. The power of the fundamental tone (7.5 GHz) of the photocurrent of LD3 is controlled to −27.53 dBm. By adjusting TODL3, a phase difference of π can be made to eliminate the second-order harmonic in Fig. 8(a). The second-order harmonic is suppressed by 35.82 dB. The power spectrum and time-domain waveform of the generated triangular waveform are shown in Fig. 8(c) and (d). The RMSE between the measured waveform and the ideal waveform is 0.0396. A triangular waveform is generated successfully.

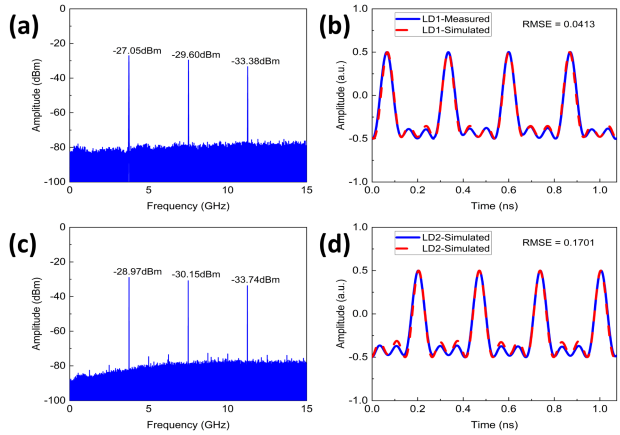

Fig. 9. (a) and (b) The power spectrum and time-domain waveform of branch-1. (c) and (d) The power spectrum and time-domain waveform of branch-2.

B. Rectangular Waveform

The Fourier expansion of a rectangular waveform can be expressed as:

$$T_{tri}(t) = C_0 + \sum_{n=1,3,5,\ldots}^{\infty} \frac{1}{n}\sin[n(\omega t+\varphi)]$$
$$\approx C_0 + \cos(\omega t+\varphi) - \frac{1}{3}\cos[3(\omega t+\varphi)] \quad (15)$$

To obtain a rectangular waveform, the ratio (3:1) of the amplitude of the fundamental tone and the third-order harmonic should be satisfied. The phase difference of π between the fundamental tone and the third-order harmonic need to be controlled.

By controlling the power of RF1, the bias current of LD1 and LD2, and the attenuator of branch-1 and branch-2, the measured power spectrum and time domain waveforms of branch-1 and branch-2 are shown in Fig. 9. HPIRPs of branch-1 and branch-2 can be obtained by least squares curve fitting as: $\psi_{12} = 0.0216rad$, $\psi_{13} = 0.0684rad$, $\psi_{22} = -0.0344rad$, $\psi_{23} = -0.0181rad$.

A simulated photonic rectangle waveform can be obtained by making $\tau_2 = \tau_1 + [(2n+1)\pi + 1.4137]/\omega_m$. The photocurrent can be expressed as:

$$\begin{cases} i_{fund} = a_{11}\cos[\omega_m(t-\tau_1)] - a_{21}\cos[\omega_m(t-\tau_1) - 1.4137] \\ i_{thir} = a_{13}\cos[3\omega_m(t-\tau_1) + 0.0684] - a_{23}\cos[3\omega_m(t \\ \qquad -\tau_1) + 4.223] \\ i_{tri} = i_{fund} + i_{thir} \end{cases} \quad (16)$$

The simulated waveforms can be seen in Fig. 10. The amplitude ratio of the fundamental tone and the third-order harmonics is 2.78, which is close to the ideal value of 3. The phase difference between fundamental tone and third-order harmonics is 0.97π, which is close to the ideal value of π. The RMSE between the simulated rectangular waveform and the ideal waveform is 0.1779. A simulated rectangular waveform is generated.

By properly adjusting the TODL of branch-2, the delay time of$\tau_2 = \tau_1 + [(2n+1)\pi + 1.4137]/\omega_m$ can be satisfied. The

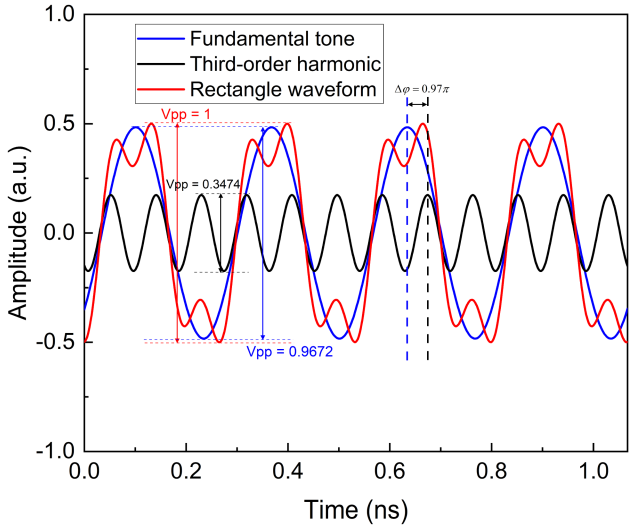

Fig. 10. The simulation of photonic generation of a rectangular waveform.

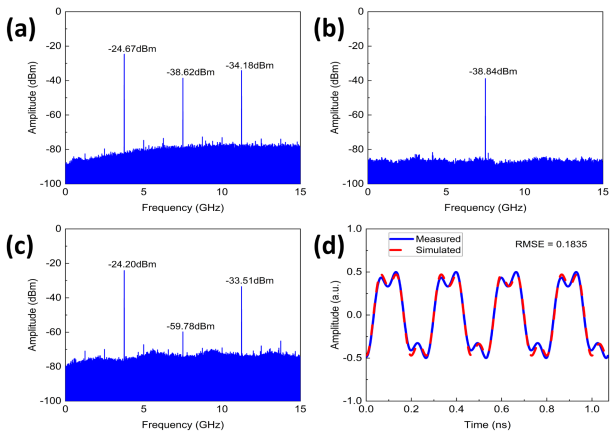

Fig. 11. (a) The power spectrum of the superposition of branch-1 and branch-2. (b) The power spectrum of branch-3. (c) The power spectrum of the superposition of the three branches. (d) The measured and simulated rectangular waveforms.

second-order harmonic can be suppressed by 35.55 dB, by controlling the phase and amplitude of the photocurrent of branch-3. The power of fundamental tone is 9.31 dB larger than that of the third-order harmonic, which is close to the theoretical value of 9.54 dB. As shown in Fig. 11(d), a target rectangular waveform is obtained. The RMSE between the measured waveform and the ideal waveform is 0.1835. The derivation of the measured waveform mainly comes from the phase-mismatch between the fundamental tone and the third-order harmonic, as analyzed in Fig. 10.

V. Conclusion

In this paper, we theoretically and experimentally analyze the harmonic-phase of photocurrent introduced by the round-trip phase of the DFB laser. When the DFB laser is under amplitude modulation, HPIRP will reduce with the increasing of modulation depth at a fixed frequency. And the HPIRP of the second-order harmonic is smaller than that of the third-order harmonic. By properly designing, the HPIRP can be controlled to generate optical microwave waveforms. A simple method for optical microwave waveforms generation based on directly modulated DFB lasers is proposed and experimentally verified. By controlling the amplitude and phase of the photocurrent of the three lasers, the photocurrent superimposed by the three branches can be equivalent to the Fourier series of a target waveform. Neither dispersive elements are required in this experiment, nor complex microwave photonic filtering is required. The amplitude and phase of the harmonics can be adjusted at the same time, which can generate the target waveform more accurately. In this scheme, photonic triangular and rectangular waveforms with a repetition rate of 3.75 GHz are successfully generated.

Acknowledgment

The authors declare no conflicts of interest.

References

[1] S. T. Cundiff and A. M. Weiner, "Optical arbitrary waveform generation," *Nature Photon.*, vol. 4, no. 11, pp. 760–766, 2010.
[2] J. P. Yao, "Photonic generation of microwave arbitrary waveforms," *Opt. Commun.*, vol. 284, no. 15, pp. 3723–3736, 2011.
[3] A. I. Latkin, S. Boscolo, R. S. Bhamber, and S. K. Turitsyn, "Doubling of optical signals using triangular pulses," *J. Opt. Soc. Amer. B*, vol. 26, no. 8, pp. 1492–1496, 2009.
[4] G.-F. Bai et al., "Versatile photonic microwave waveforms generation using a dual-parallel Mach–Zehnder modulator without other dispersive elements," *Opt. Commun.*, vol. 396, pp. 134–140, 2017.
[5] H. Chen and J. Ma, "Photonic generation of flexible and adjustable microwave waveforms based on a dual-polarization Mach–Zehnder modulator," *Appl. Opt.*, vol. 60, no. 27, pp. 8299–8306, 2021.
[6] C. Wang et al., "Photonic generation of frequency-quadrupled triangular waveform based on a DP-QPSK modulator with tunable modulation index," *Opt. Laser Technol.*, vol. 137, 2021, Art. no. 106818.
[7] S. Zhu, X. Wang, M. Li, N. H. Zhu, and W. Li, "A simple photonic method to generate square and triangular microwave waveforms," *Opt. Commun.*, vol. 426, pp. 654–657, 2018.
[8] X. Chen et al., "Photonic generation of rectangular and triangular microwave waveforms with tunable duty cycle," *IEEE Photon. Technol. Lett.*, vol. 34, no. 7, pp. 371–374, Apr. 2022.
[9] Y. He et al., "Photonic microwave waveforms generation based on two cascaded single-drive Mach-Zehnder modulators," *Opt. Exp.*, vol. 26, no. 6, pp. 7829–7841, 2018.
[10] L. Xie et al., "24-GHz directly modulated DFB laser modules for analog applications," *IEEE Photon. Technol. Lett.*, vol. 24, no. 5, pp. 407–409, Mar. 2012.
[11] S. Matsuo and T. Kakitsuka, "Low-operating-energy directly modulated lasers for short-distance optical interconnects," *Adv. Opt. Photon.*, vol. 10, no. 3, pp. 567–643, 2018.
[12] J. Wang, Y. Huang, Y. Liu, H. Zhu, L. Xie, and Q. Kan, "Low harmonic distortion DFB laser for broadband analog applications," *IEEE Photon. Technol. Lett.*, vol. 32, no. 14, pp. 887–890, Jul. 2020.
[13] N. Otsuka, M. Kito, M. Ishino, and Y. Matsui, "1.5-μm strained-layer MQW-DFB lasers with high relaxation-oscillation frequency and low-chirp characteristics," *IEEE J. Quantum Electron.*, vol. 32, no. 7, pp. 1230–1236, Jul. 1996.
[14] H. Haisch et al., "Low-chirp highly linear 1.55 mu m strained-layer MQW DFB lasers for optical analog TV distribution systems," *IEEE J. Quantum Electron.*, vol. 29, no. 6, pp. 1782–1791, Jun. 1993.
[15] W. Liu and J. Yao, "Photonic generation of microwave waveforms based on a polarization modulator in a Sagnac loop," *J. Lightw. Technol.*, vol. 32, no. 20, pp. 3637–3644, Oct. 2014.